Ceramics International xxx (xxxx) xxx–xxx

Contents lists available at ScienceDirect

Ceramics International

journal homepage: www.elsevier.com/locate/ceramint

Combustion synthesis and characterization of $Ln_{1-x}M_xCr_{0.9}Ni_{0.1}O_3$ (Ln = La and/or Nd; M = Sr and/or Ca; x ≤ 0.25) perovskites for SOFCs anodes

L. Ortega-San-Martín[a,*], A. Morán-Ruiz[b], A. Wain-Martin[b], K. Vidal[b,*], A. Larrañaga[b], M.A. Laguna-Bercero[c], M.I. Arriortua[b,d,**]

[a] Departamento de Ciencias, Sección Química, Pontificia Universidad Católica del Perú (PUCP), Av. Universitaria 1801, Lima 32, Peru
[b] Facultad de Ciencia y Tecnología, Universidad del País Vasco/Euskal Herriko Unibertsitatea (UPV/EHU), Sarriena s/n, 48940 Leioa, Spain
[c] CSIC-Universidad de Zaragoza, Instituto de Ciencia de Materiales de Aragón (ICMA), Pedro Cerbuna 12, 50009 Zaragoza, Spain
[d] BCMaterials, Parque Tecnológico de Zamudio, Ibaizabal Bidea, Edificio 500- Planta 1, 48160 Derio, Spain

ARTICLE INFO

Keywords:
Chemical synthesis
Electrical conductivity
SOFC
Anode
A-site

ABSTRACT

A series of chromite perovskites with the general formula $Ln_{1-x}M_xCr_{0.9}Ni_{0.1}O_3$ (Ln = La and/or Nd; M = Sr and/or Ca; x ≤ 0.25) has been prepared by three combustion synthesis routes using a different combustible substance each time: glycine, urea and sucrose. In order to isolate the effect of divalent dopant concentration from the A cation steric effects, the whole group has a fixed mean A cation radius, $< r_A > \approx 1.22$ Å, and cation size disorder, $\sigma^2(r_A) \approx 0.0001$ Å^2, but variable doping x. Their crystal structure, microstructure, electrical properties and expansion coefficients have been investigated on the basis of their possible use as anode materials for intermediate temperature solid oxide fuel cells (SOFC). Cell parameters, grain sizes, expansion coefficients and conductivities all are found to be dependent on x and the combustible substance used. The most interesting relationship is the negative dependence of the conductivity with x under H_2 atmosphere: conductivity decreases with doping which is the opposite to the expected behavior for a p-type doped perovskites and has not been reported before.

1. Introduction

The research to find new or to improve the most commonly used materials in solid oxide fuel cells (SOFC) is still a important field in materials science [1]. In particular, one of the most active area is the study of SOFC anodes because the operation of commercial SOFC devices is strongly dependent on the behavior of this electrode, which is in contact with the fuel (and all its impurities) [2]. The number of materials studied as possible anodes is huge and, among them, perovskites have also gained attraction due to their good catalytic properties, high ionic and electrical conductivities, and their chemical and thermal stabilities at high temperatures.

The main concern for current nickel-yttria stabilized zirconia cermet anodes is that they are unable to work efficiently with hydrocarbon fuels at intermediate operating temperature range (600–800 °C) due to their sulfur content and also as a consequence of carbon deposition [3]. Hence, there is still a demand for the development of alternate anode materials with improved tolerance towards carbon deposition and sulfur poisoning to improve the fuel flexibility and efficiency of SOFCs.

Oxide-perovskites have been widely studied as possible cathode electrodes for a long time due to their mixed ionic and electronic conductivity (MIEC), high catalytic activity and good stability under oxidizing conditions [1,4]. To be used as anodes, however, perovskites need to be stable under reducing conditions. Among the oxide perovskites that have good catalytic properties and appropriate MIEC, only chromites are reasonably stable in reducing atmospheres and this is why they have been thoroughly investigated as SOFC-interconnectors [5] and also proposed as possible anodes [6–11]. From the thermodynamic point of view, chromites are expected to react with the common YSZ electrolyte but in practice, this only occurs to a great extent at temperatures above the operation ones (that is, higher than 1000 °C) [12].

When a material is evaluated as a SOFC component, it is also important to consider its preparation costs. Perovskites are usually prepared at high temperatures so another important field of research is aimed at reducing energy consumption of the synthesis [13]. Combustion synthesis routes, which involve low cost materials, short processing time and produce large amount of gases that inhibit particle size

* Corresponding authors.
** Corresponding author at: Facultad de Ciencia y Tecnología, Universidad del País Vasco/Euskal Herriko Unibertsitatea (UPV/EHU), Sarriena s/n, 48940 Leioa, Spain.
E-mail addresses: lortegas@pucp.edu.pe (L. Ortega-San-Martín), karmele.vidal@ehu.es (K. Vidal), maribel.arriortua@ehu.es (M.I. Arriortua).

http://dx.doi.org/10.1016/j.ceramint.2017.10.182
Received 30 August 2017; Received in revised form 23 October 2017; Accepted 25 October 2017

Table 1
Nominal stoichiometries, mean radii and A-site disorder values of the $Ln_{1-x}M_xCr_{0.9}Ni_{0.1}O_3$ perovskites.

x	$Ln_{1-x}M_xCr_{0.9}Ni_{0.1}O_3$	$< r_A >$ (Å)	$\sigma^2(r_A)$ (Å^2)*
0.10	$La_{0.85}Nd_{0.05}Sr_{0.10}Cr_{0.90}Ni_{0.10}O_3$	1.22	0.00010
0.15	$La_{0.80}Nd_{0.05}Sr_{0.10}Ca_{0.05}Cr_{0.90}Ni_{0.10}O_3$	1.22	0.00011
0.20	$La_{0.80}Sr_{0.10}Ca_{0.10}Cr_{0.90}Ni_{0.10}O_3$	1.22	0.00011
0.25	$La_{0.75}Sr_{0.10}Ca_{0.15}Cr_{0.90}Ni_{0.10}O_3$	1.22	0.00011

* Cation size disorder has been calculated using the equation $\sigma^2(r_A) = < r_A^2 > - < r_A >^2$ and ninefold coordination radii for the A-site cations (see text).

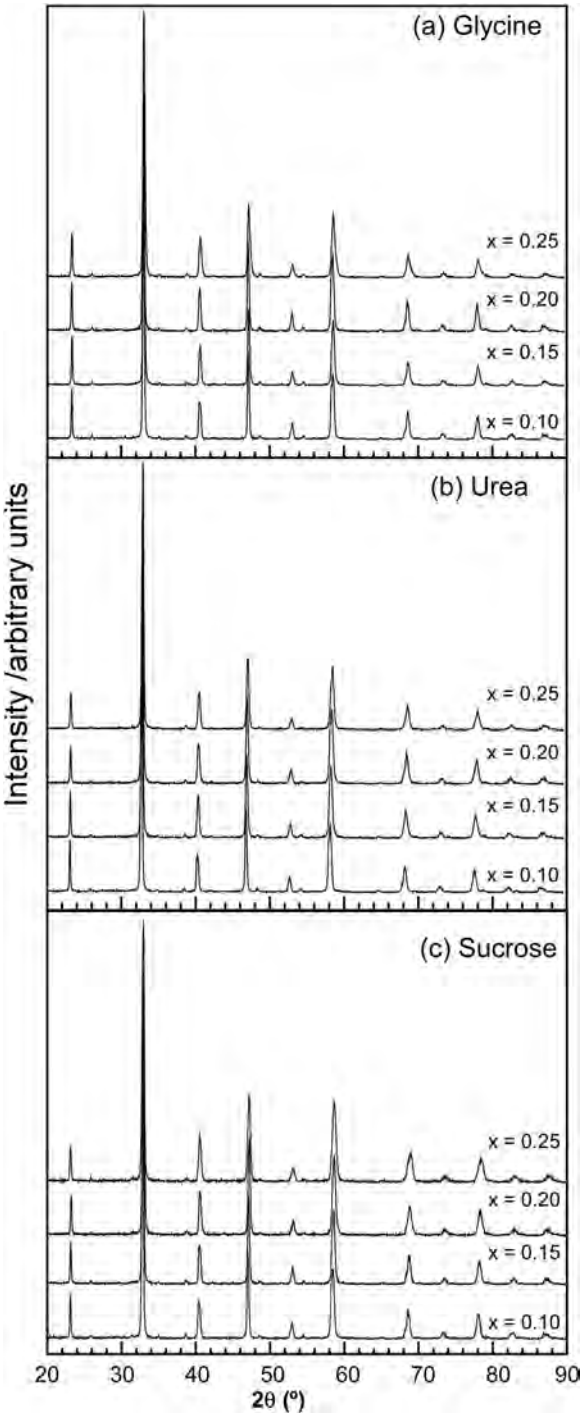

Fig. 1. X-ray diffraction patterns for the series $Ln_{1-x}M_xCr_{0.9}Ni_{0.1}O_3$ (Ln = La and/or Nd; M = Sr and/or Ca; x ≤ 0.25) prepared using (a) glycine, (b) urea and (c) sucrose as combustible agents.

Table 2
Summary of the ICP results for the $Ln_{1-x}M_xCr_{0.9}Ni_{0.1}O_3$ perovskites.

x	Fuel	$Ln_{1-x}M_xCr_{0.9}Ni_{0.1}O_3$
0.10	Glycine	$La_{0.86(1)}Nd_{0.04(1)}Sr_{0.11(1)}Cr_{0.90(2)}Ni_{0.10(1)}$
	Urea	$La_{0.87(1)}Nd_{0.05(1)}Sr_{0.10(1)}Cr_{0.90(2)}Ni_{0.11(1)}$
	Sucrose	$La_{0.85(1)}Nd_{0.05(1)}Sr_{0.11(1)}Cr_{0.90(2)}Ni_{0.11(1)}$
0.15	Glycine	$La_{0.76(1)}Nd_{0.04(1)}Sr_{0.11(1)}Ca_{0.07(1)}Cr_{0.90(1)}Ni_{0.10(1)}$
	Urea	$La_{0.78(1)}Nd_{0.05(1)}Sr_{0.10(1)}Ca_{0.05(1)}Cr_{0.90(1)}Ni_{0.10(1)}$
	Sucrose	$La_{0.81(1)}Nd_{0.06(1)}Sr_{0.10(1)}Ca_{0.06(1)}Cr_{0.90(1)}Ni_{0.10(1)}$
0.20	Glycine	$La_{0.82(1)}Sr_{0.10(1)}Ca_{0.09(1)}Cr_{0.90(2)}Ni_{0.10(1)}$
	Urea	$La_{0.80(1)}Sr_{0.10(1)}Ca_{0.11(1)}Cr_{0.90(2)}Ni_{0.10(1)}$
	Sucrose	$La_{0.81(1)}Sr_{0.11(1)}Ca_{0.10(1)}Cr_{0.90(2)}Ni_{0.11(1)}$
0.25	Glycine	$La_{0.74(1)}Sr_{0.08(2)}Ca_{0.16(1)}Cr_{0.90(2)}Ni_{0.11(1)}$
	Urea	$La_{0.75(1)}Sr_{0.09(2)}Ca_{0.15(1)}Cr_{0.90(2)}Ni_{0.10(1)}$
	Sucrose	$La_{0.75(1)}Sr_{0.11(1)}Ca_{0.13(1)}Cr_{0.89(2)}Ni_{0.10(1)}$

growth, are of great interest in synthesizing nano-size powders with high specific surface area [14]. In this type of synthesis, the combustion velocity, the choice of the combustible substance and its amount are very important factors that influence the final properties of the obtained powder [15]. The effect of the type of combustible substance on the electrochemical properties of SOFC materials has not been investigated in detail and, consequently, its role is unclear [16].

In this study, we investigate two effects: (i) the variation of the doping level x and (ii) the use of different combustible substances (glycine, urea and sucrose) during the synthesis by the combustion method in the structure and electrical properties of a series of new chromite perovskites with the formula $Ln_{1-x}M_xCr_{0.9}Ni_{0.1}O_3$ (Ln = La and/or Nd; M = Sr and/or Ca; x ≤ 0.25). To avoid the interplay of different A-site variables in their properties the mean ionic radius $< r_A >$ (1.22 Å) and the cation size disorder $\sigma^2(r_A)$ (0.0001 Å^2) have been kept constant. To meet these requirements up to four different A cations were used in the same oxide. Low disorder has been selected from previous studies which showed that the higher the disorder the lower the performance of the oxides irrespective their field of application [17–21]. On the other hand, the chemical compositions have been selected bearing in mind the maximum solubility of calcium and strontium in chromites (x < 0.3 for both of them) and considering that they had to contain strontium as its presence improves the stability of the perovskite under low oxygen partial pressures [12]. X-ray powder diffraction (XRD), scanning electron microscopy (SEM), electrical measurements and thermal expansion studies have been also carried out.

2. Experimental

2.1. Powder preparation

$Ln_{1-x}M_xCr_{0.9}Ni_{0.1}O_3$ samples were prepared by combustion synthesis using $La(NO_3)_3{\cdot}6H_2O$ (> 99%), $Nd(NO_3)_3{\cdot}6H_2O$ (99.9%), $Sr(NO_3)_2$ (99.99%), $Ca(NO_3)_2{\cdot}H_2O$ (99.997%), $Ni(NO_3)_2{\cdot}6H_2O$ (99.999%) and $Cr(NO_3)_3$ (> 99%) as metal precursors and glycine, urea and sucrose (all from Aldrich, > 99%) as combustible substances. The prepared compositions, together with their mean ionic radius, $< r_A >$, and A cation size disorder, $\sigma^2(r_A)$, are summarised in Table 1. It is to note that disorder (quantified as $\sigma^2(r_A) = < r_A^2 > - < r_A >^2$) has been calculated using ninefold coordination radii for the A site cations [22] in order to be consistent with previous literature data and because this is the expected coordination for an orthorhombic perovskite [23] such as the parent $LaCrO_3$ [24].

The metal nitrates were dissolved in distilled water. The solutions (dissolved metal nitrates) were mixed in a glass beaker, which was placed on a hot plate at 100 °C to evaporate excess water under constant stirring. Then, the glycine, urea or sucrose was added to obtain a molar ratio of 1 with the oxidizer. The resulting viscous liquid started autoignition just after placing the glass beaker directly onto a preheated

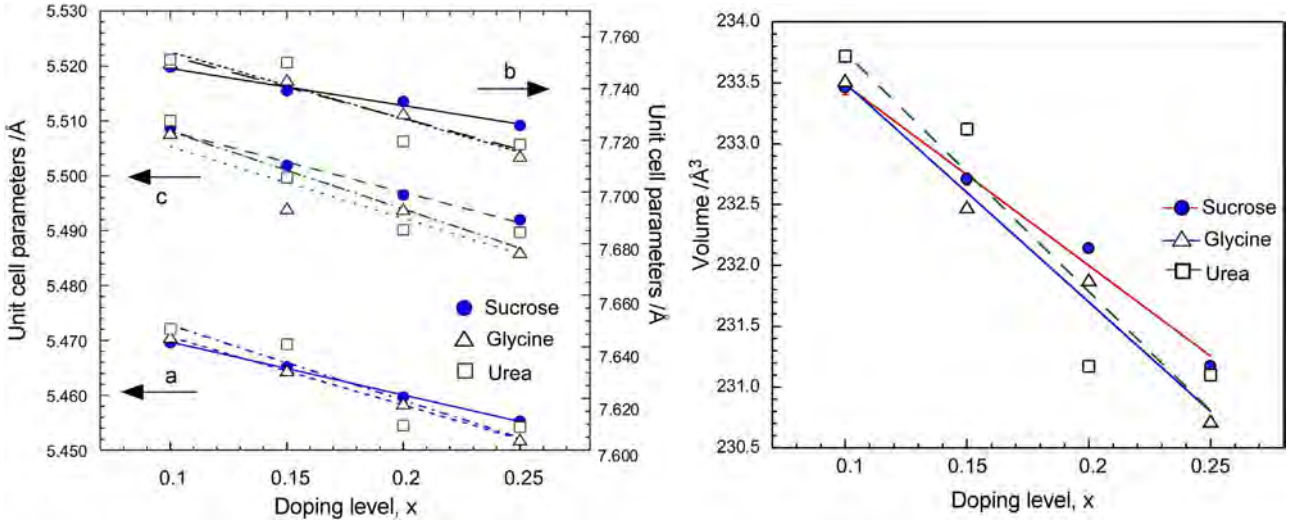

Fig. 2. Variation of the unit cell parameters and volume with doping for the samples obtained using different fuels. Lines are linear fits in all cases.

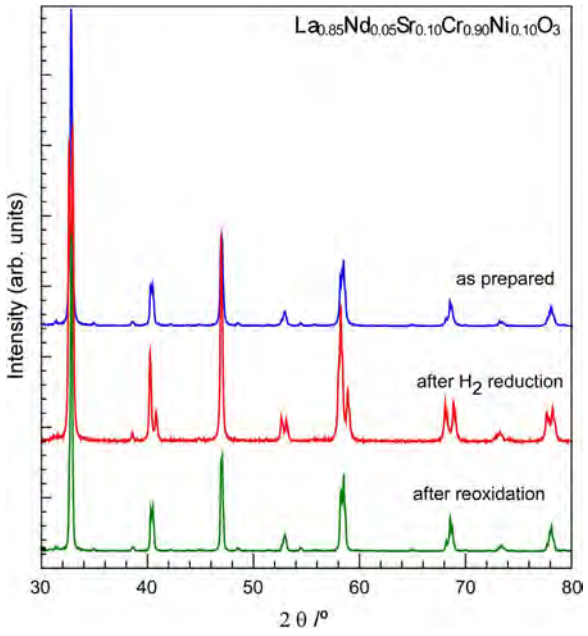

Fig. 3. Comparison of the XRD data taken for x = 0.1 phase under different atmosphere conditions: as –synthesised, after H_2-conductivity test and after reoxidation in air.

plate (at 350 °C). The obtained powders were calcined at 800 °C for 2 h to remove the carbon residues and, after that, these samples were pressed at 45 MPa to form 13 mm diameter pellets by a manual hydraulic press. Pellets were calcined in air for 10 h at temperatures up to 1200 °C until pure samples were obtained. This was achieved after two or three repetitions, the samples being ground and pelletised again for each calcination step.

2.2. Characterization techniques

The structural analysis was performed using laboratory X-ray diffraction (XRD). XRD data were collected from 15 to 90° in 2θ with an integration time of 500 s/0.026° step using a Philips X'Pert-PRO X-ray diffractometer using copper Kα radiation without Ni-filter and a PIXcel solid state detector (active length in 2θ 3.347°). A fixed divergence and antiscattering slit giving a constant volume of sample illumination were used. The crystal structure was refined by the Rietveld method using the GSAS software package [25] and EXPGUI interface [26].

All metal contents were determined by inductively coupled plasma atomic emission spectroscopy (ICP-AES) on a Horiba Yobin Yvon Activa spectrophotometer. For this purpose, samples were dissolved using a mixture of HNO_3 and HCl for two days to obtain a clear and measurable solution.

Prior to bulk conductivity and dilatometry measurements pellets of the as-synthesised powders were sintered at 1350 °C for 10 h and, subsequently, cut into rectangular bars. The bulk density of each sample was estimated by measuring the mass and the dimensions of the bars using a digital micrometer (Mitutoyo, Japan). DC conductivity measurements were performed under pure H_2 by the four-point DC method from 800 to 400 °C using a VSP potentiostat controlled by PC using Lab Windows/CVI field point system. Electrical contacts were made using Pt wires and Pt paste placed over whole end faces ensuring a homogeneous current flow. Prior to the start of the measurements, each oxide was kept at 800 °C for 12 h under flowing H_2 at a rate of 120 ml/min (oxygen partial pressure nearly 10^{-21} atm). Conductivity data were corrected considering the experimental density values (all around 85% of the theoretical (X-ray) density).

Thermal expansion coefficients were measured from room temperature to 950 °C under air with a heating rate of 5 °C min^{-1} using a Unitherm Model 1161 dilatometer. Morphologies of the as-synthesised powder samples and the sintered pellets were observed using a scanning electron microscope (JEOL JSM-7000F). Secondary electron images were taken at 20 kV and 1.1.10^{-11} A.

3. Results and discussion

3.1. Structural study

Room temperature X-ray diffraction patterns of all as-synthesised oxide perovskites are shown in Fig. 1. The patterns reveal that all the samples are single-phase and no impurities are detected within the resolution limits of the used technique.

Results from chemical analyses, presented in Table 2, show a good agreement between the analysed chemical compositions of the prepared powders and the nominal compositions.

Rietveld fits to the powder X-ray diffraction data were carried out using the orthorhombic (*Pnma*) space group, the same observed for the parent $LaCrO_3$ phase at room temperature [24], considering the nominal composition in the different sites of the crystal structure. Only three independent thermal parameters were used in the refinements (one for the A-site cations, another for the B-site ones and a final one for all the oxygen atoms). Graphs of the Rietveld fits to all the oxides

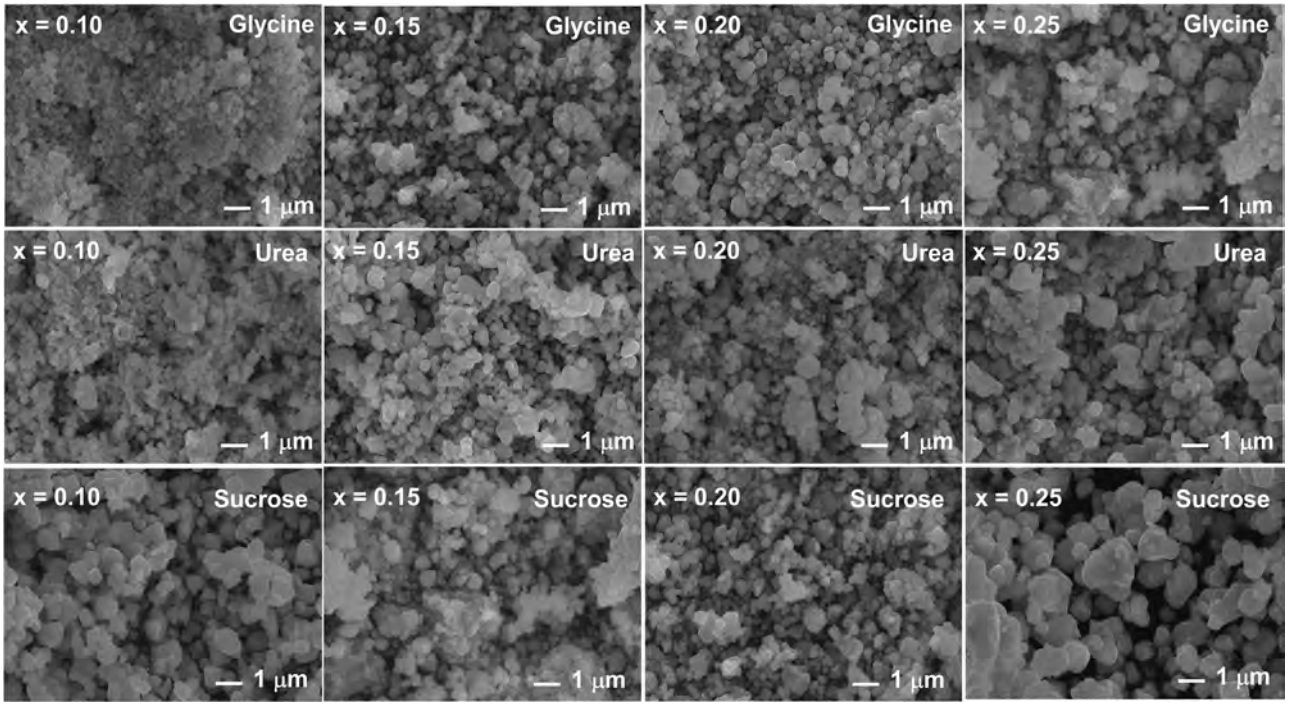

Fig. 4. SEM micrographs of $Ln_{1-x}M_xCr_{0.9}Ni_{0.1}O_3$ perovskites calcined between 1100 and 1200 °C.

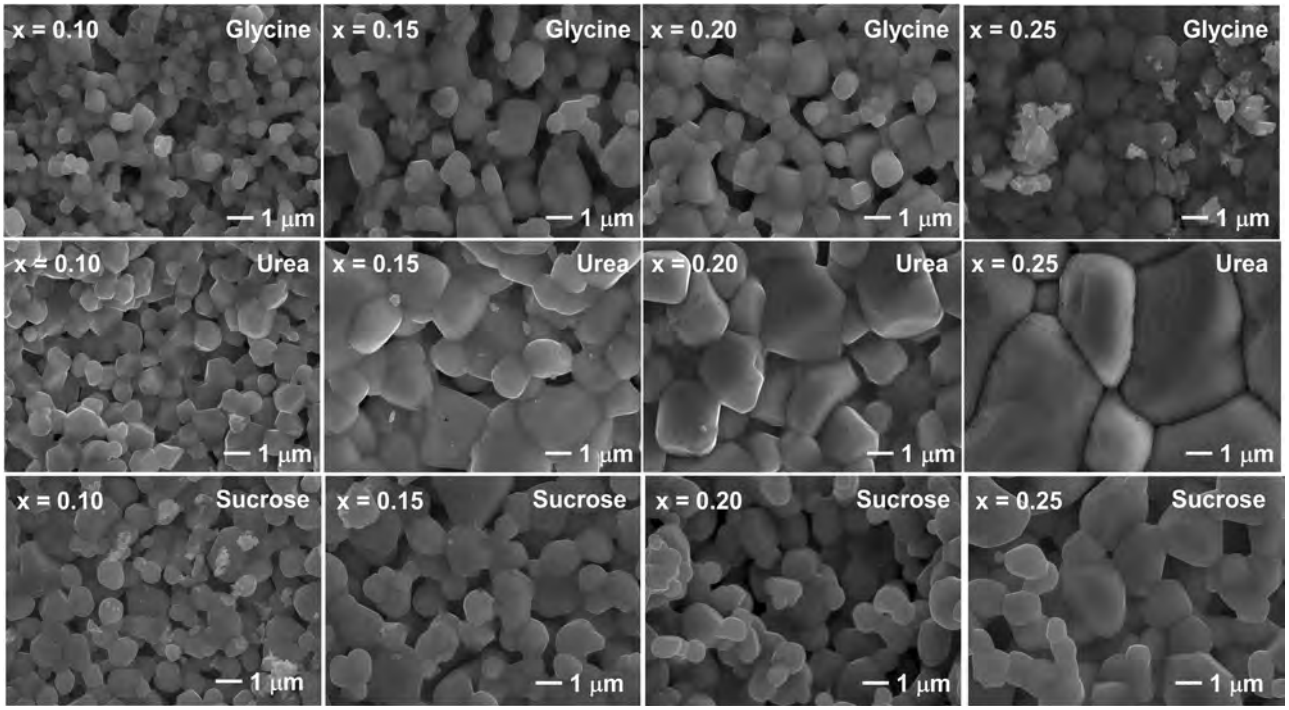

Fig. 5. SEM micrographs taken on the surface of the pellets sintered at 1350 °C in air for 10 h.

prepared are shown in supplementary Figs. S1–S3.

The variation of the unit cell parameters and cell volume with doping (x) is shown in Fig. 2. As it can be observed, there is a systematic decrease in volume with increasing divalent dopant content. This behavior cannot be associated with changes in the A position because the variables that influence lattice volume, such as the A-site mean ionic radius $< r_A >$ and the A-site disorder [27], have been kept constant throughout the series. Therefore, the observed decrease of the lattice parameters can be only associated with the reduction of the B-site (chromium and nickel) mean ionic radii ($< r_B >$) as a consequence of their oxidation with the increase of the doping level x (the ionic radii in octahedral coordination of Cr and Ni decrease from $r_{(Cr3+)} = 0.615$ Å and $r_{(Ni2+)} = 0.69$ Å to $r_{(Cr4+)} = 0.55$ Å, and $r_{(Ni3+)} = 0.56$ Å, respectively) [22].

The structural parameters, atomic distances and R factors obtained by Rietveld refinement to the X-ray data of all the compounds obtained using the different combustible substances are displayed in Tables S1–S3 of the supplementary information. According to our data, there are not many structural variations along the series with doping apart from the compression of the unit cell, as expected.

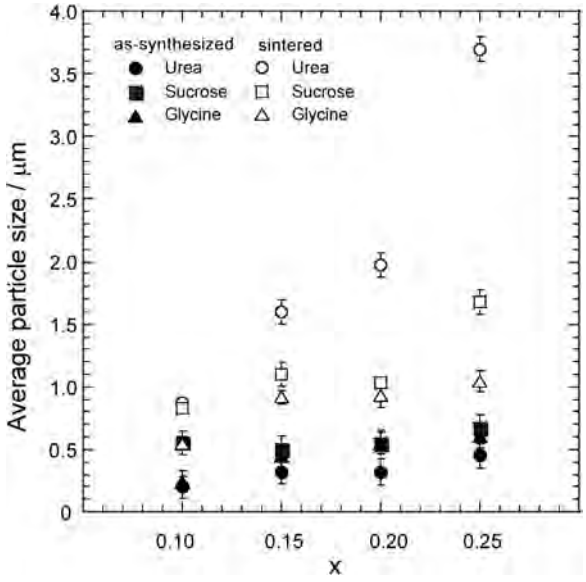

Fig. 6. Doping and fuel dependence of the average particle sizes calculated from SEM images.

The crystal structure of the oxides was also studied after the conductivity measurements that were carried out under hydrogen atmosphere in order to establish the stability of the samples. It is interesting to note that the room temperature XRD data showed that none of the samples degraded and all were single phase after the treatment but with a different crystal structure: data were fitted to a *R*-3*c* distorted perovskite. This indicates that the oxides retain the high temperature phase of the parent $LaCrO_3$ which experiments a *Pnma* → *R*-3*c* phase transition above 250 °C [24]. This higher symmetry structure is probably a result of the rearrangement of the atoms that resulted from the oxygen loss at temperatures between 400–800 °C. Nevertheless, the initial crystal structure is fully recovered after the oxides are heated again in air at 800 °C. Fig. 3 shows the x = 0.1 oxide prepared using sucrose as a representative example. No impurities are observed after this cycle which further supports that these oxides are thermally stable as expected for anode perovskites.

3.2. Morphological study

Representative SEM micrographs of the powder samples obtained by the combustion method using glycine, urea and sucrose after final calcination (as-synthesised powders) are shown in Fig. 4.

These powders are composed of agglomerates formed by very small size particles. The average size of the grains calculated by direct SEM observation ranges from 200 to 250 nm observed for the x = 0.10 oxide prepared using glycine to 550–600 nm observed for the x = 0.25 phase prepared using sucrose. It is interesting to note that the average particle size slightly increases with x irrespective of the synthesis method, being the x = 0.25 oxides the ones that show the biggest grain sizes.

Usually, smaller crystallite sizes are formed when the combustion temperature is not very high and, specially, when a large volume of gases is evolved because this further enhances the dissipation of heat and limits the inter-particle contact, preventing grain growth. The comparison of combustible substances in the literature [15,28,29], however, are not definitive regarding to which one results in smaller particles mainly because each author uses different combustible to oxidizer ratios, which has a strong influence on the combustion temperature [30], so those results are not easily comparable. In the present case, our results indicate that glycine and urea combustion yield smaller particles than sucrose probably because non-nitrogen containing combustibles are not as efficient dissipating the combustion temperature

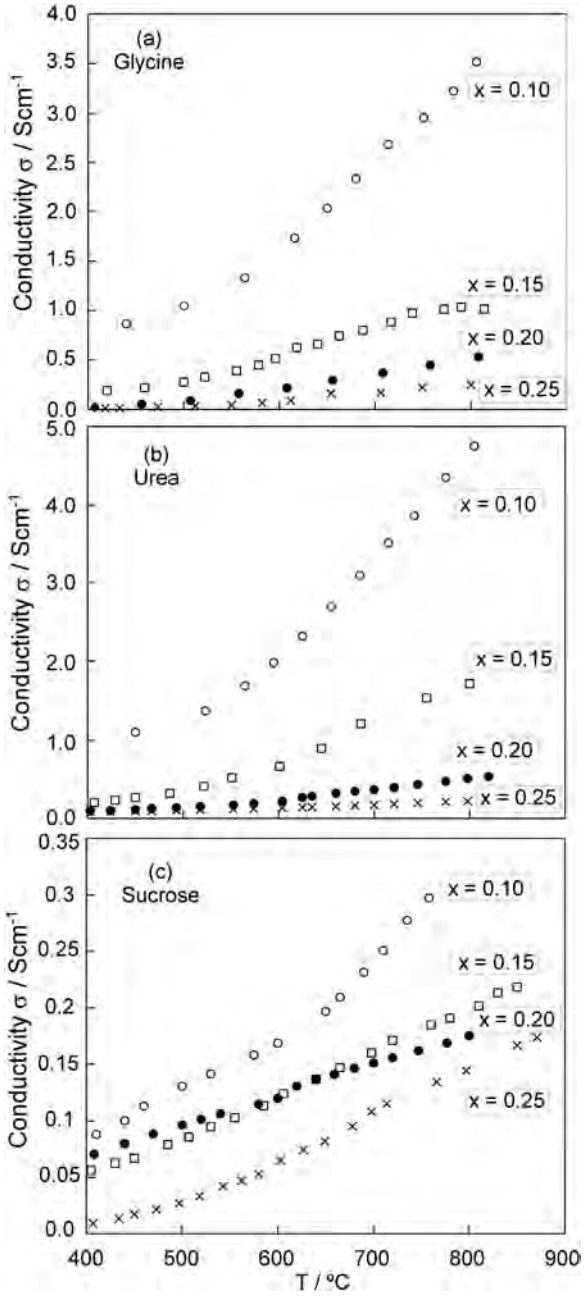

Fig. 7. Conductivity dependence upon temperature as a function of x measured in H_2 for the oxides prepared using (a) glycine, (b) urea and (c) sucrose as combustible agents.

than the nitrogen ones.

On the other hand, the increase of grain size with x can be related to the calcium content in the phases. Several studies have shown that the addition of calcium to $LaCrO_3$ allows the formation of a transient liquid phase due to the formation of $CaCrO_4$, specially above 1150 °C, resulting in sintered microstructures with bigger particle sizes and denser ceramics [31,32].

After sintering at 1350 °C in air for 10 h the trends in particle sizes are maintained, as observed in the SEM images shown in Fig. 5: the higher the x (calcium content) the biggest the particle sizes. As expected, this also resulted in denser materials with x: from the lowest to the highest doping, the relative densities increased from 60% to 88%, from 76% to 95% and from 70% to 92% of the theoretical XRD-values for the perovskites synthesised using glycine, urea and sucrose, respectively.

Fig. 5 also shows that, after sintering, all oxides present bigger

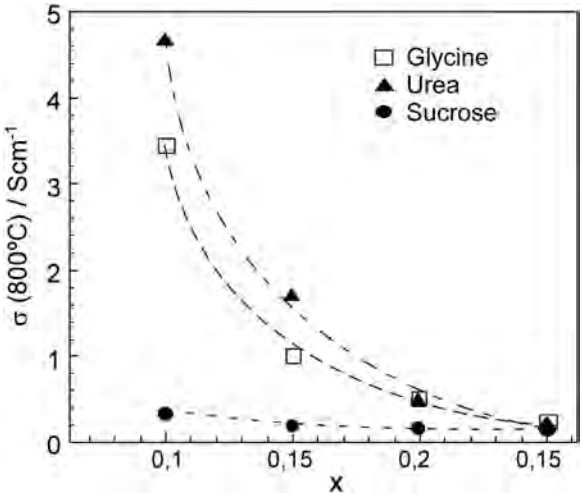

Fig. 8. Doping dependence of the conductivity at 800 °C measured under reducing conditions. Lines are guides for the eyes.

particle sizes compared to the as-synthesised powders, which is an expected result, but the increase is dependent on the synthesis method, being the samples prepared by the urea combustion process the ones that show the biggest increase (near tenfold for the x = 0.25 oxide). Fig. 6 summarises the observed tendencies. This difference in the sintering behavior is probably a result of the different agglomeration that results from the combustion. According to the literature [33], this seems to indicate that the as-synthesised urea powders presented softer agglomerates which could be broken during cold-pressing to enhance number of contact points. A more detailed study of the sintering behavior (using different firing temperatures, for example) would be necessary, however, to know if this behavior is maintained in all cases, but this is beyond the scope of this work.

3.3. Electrical conductivity study

The total electrical conductivity, σ, measured under H_2 atmosphere of all the sintered $Ln_{1-x}M_xCr_{0.9}Ni_{0.1}O_3$ perovskites as function of doping level x from 400 to 800 °C is shown in Fig. 7. A summary of the data at 800 °C for all the studied compounds appears in Fig. 8.

It can be clearly seen that the conductivity is strongly dependent on both the preparation route and the doping level. In all cases the oxides prepared by the urea combustion route show higher conductivity values than the glycine and sucrose oxides. It is interesting to note that the maximum conductivity values of the glycine and urea samples with x = 0.1 and 0.15 are above the minimum of 1 S cm^{-1} expected for an oxide anode [34] and higher than many of the previously reported values of similar $Ln_{1-x}A'_xCr_{1-y}M_yO_{3-d}$ compounds at low oxygen partial pressures [35–39]. The sucrose samples, however, show conductivity values that are roughly an order of magnitude smaller and below those expected for anode applications.

The most important feature of the electrical behavior of these samples is, however, the conductivity dependence on the doping value x. As observed, it follows the opposite trend that would be expected for these oxides: the conductivity decreases as the doping increases and this occurs irrespective of the synthesis process followed. This is interesting because, under air, this type of oxides show a p-type conductivity mainly based on the hoping process between Cr^{4+} and Cr^{3+} (together with some Ni^{2+} – Ni^{3+} exchange, in this case). The conducting mechanism when x increases is well known: as the alkaline-earth ions are introduced in the A-site to substitute the rare earth ions the concentration of electronic holes (mainly Cr^{4+}, but also some Ni^{3+} in the present case) increases to compensate for the smaller oxidation state of the new ions and, as a consequence, the same occurs to the p-type conductivity [40]. Under low oxygen partial pressures the formation of oxygen vacancies overrides this compensation mechanism and causes a strong reduction on the amount of holes (two Cr^{4+} ions reduce to Cr^{3+} in order to compensate for every O^{2-} ion that leaves the lattice) and this is why, in this type of oxides, conductivity under reducing conditions is always smaller than under oxidizing conditions [35–37,39–44].

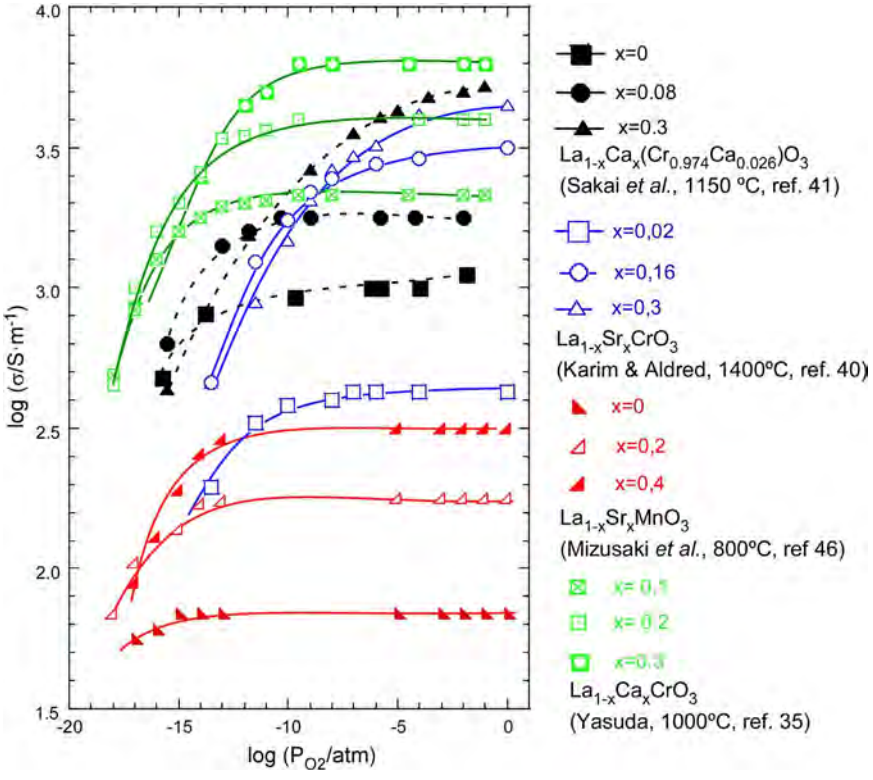

Fig. 9. Oxygen partial pressure dependence of the electrical conductivity in several doped oxides. Data taken from the literature cited. Lines are guides for the eyes. Fits are to be found in the original literature.

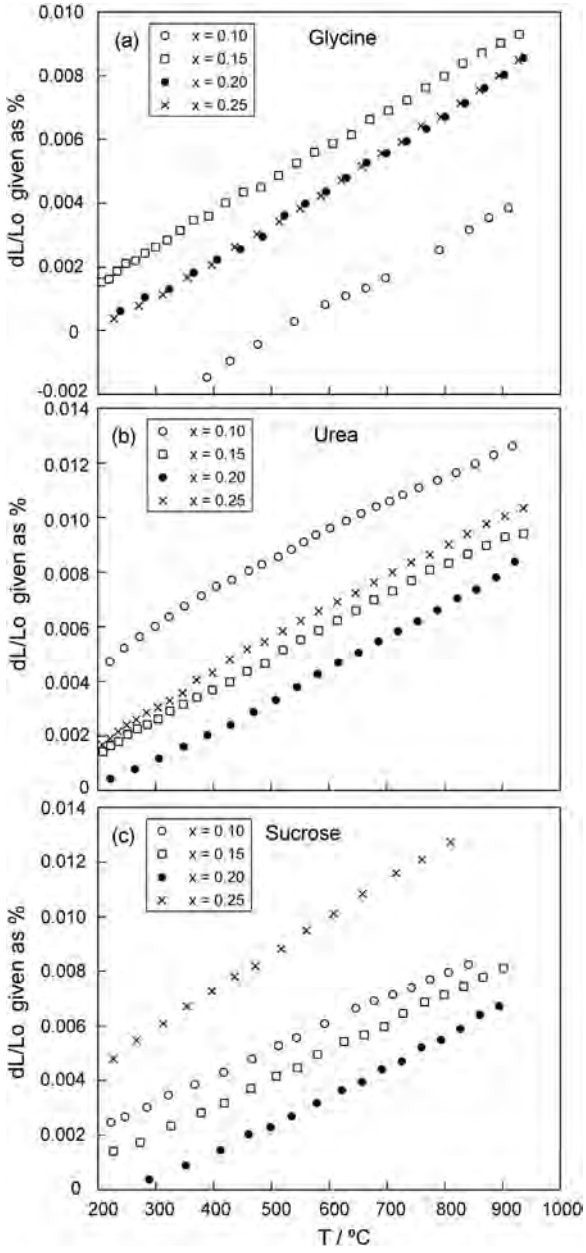

Fig. 10. Thermal expansion behavior of the $Ln_{1-x}M_xCr_{0.9}Ni_{0.1}O_3$ perovskites obtained using (a) glycine, (b) urea and (c) sucrose as fuels.

Nevertheless, if the conductivity of these oxides remained as p-type the same trend (increase of electrical conductivity) should be observed with increasing x (or y) as it has been reported in many of the previous studies of $A_{1-x}A'_xCr_{1-y}M_yO_3$ chromites [36,37,41,43,45]. However, we observe exactly the opposite behavior in all our cases irrespective of the synthesis process which indicates that this behavior is an intrinsic characteristic of the present oxides.

A thorough search of similar chromites in the literature has revealed that this behavior could also be intrinsic to other doped chromites if sufficiently low oxygen pressures are used [35,40–42]. Although, to our surprise, this negative correlation between doping and conductivity has not been noted by previous authors, data taken from their works and shown together in Fig. 9 indicate that this inversion would occur in all cases at low oxygen partial pressures. As it is observed, this behavior also occurs in doped manganites such as $La_{1-x}Sr_xMnO_3$ [46] and similar effects are encountered in $La_{1-x}Sr_xCoO_3$ cobaltites (not included in Fig. 9) [47]. All previous works coincide in two observations when

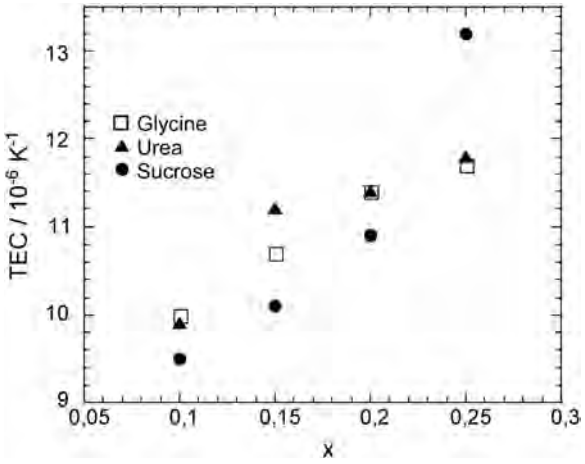

Fig. 11. Doping dependence of the thermal expansion coefficients for all samples.

these oxides are studied at low pO_2: the amount of oxygen vacancies increases more rapidly as x increases and the electric conductivity decreases in the same way [35,47,48]. The increase of oxygen vacancies is also correlated with a higher lattice expansion as pO_2 reduces [49].

Nevertheless, we have not found in the literature an explanation of why the formation of vacancies increases much faster on heavily doped oxide perovskites although this is important for the final electrical behavior. We have to rule out lattice effects coming from A-site mean ionic radii or the A-site disorder because this occurs either with them fixed (present case) and when they are left to change for every x-value (all other examples). The synthesis method seems not to be an option either because all show the same behavior (present case and in the literature). There is a correlation with the reduction of the lattice volume but it is difficult to find cause-effect relationship in this case considering that the lattice expansion, bigger for higher x, seems to override this effect at low pO_2 as indicated before [49]. What is common in all cases, including the present, is the reduction of the mean electronegativity of the A-site cations, which is systematically reduced as calcium or strontium ions substitute the more electronegative rare earths [50]. The lowering of the average electronegativity of the A-site with x might facilitate the creation of oxygen vacancies and, as a result, the reduction of conductivity is bigger in the most heavily doped oxides. At sufficiently low oxygen partial pressure this greater reduction for samples with higher x leads to an inversion of the tendency with doping: conductivity reduces with doping instead of increasing.

We consider that this is an interesting and important finding because most studies are focused, including this one, on finding the highest conductivity of a group of oxide perovskites by increasing the doping but if the conductivity is not tested at sufficiently low oxygen partial pressures (present case is $\sim 10^{-21}$ atm), the observed results might not be representative of the final behavior under SOFC operation conditions as this study shows.

3.4. Thermal expansion study

Thermal expansion measurements on rectangular bars carried out in air atmosphere upon heating from 200 to 950 °C are shown in Fig. 10a-c. The average linear thermal expansion coefficient obtained from this figure for each sample is shown in Fig. 11.

It can be seen that, although the thermal expansion coefficients (TEC) of all phases are all very similar and also agree with those of similar chromite perovskites [51], there is a small increase in TECs with increasing the doping level x in the three families of perovskites prepared.

This increase may be attributed to the formation of oxygen vacancies and the concomitant reduction of Cr^{4+} and Ni^{3+} ions with increasing x as both processes will result in lattice expansion. It is

interesting to note that the TEC values obtained for the samples with low amount of dopant are very close to those of YSZ electrolyte ($TEC_{(8YSZ;300–1000\ ^{\circ}C)} = 10.0–10.8 \times 10^{-6} K^{-1}$) [52], and those are also the phases with higher conductivity, which is quite important if these oxides were to be used as anodes. The higher expansion of the most heavily doped phases agrees with all the literature data: either under air or under low pO_2 atmosphere it is always observed that lattice expansion increases with temperature due to the increase of oxygen vacancies and, as indicated previously, given that the amount of vacancies formed increases with x, the same is expected to occur with the thermal expansion coefficients.

4. Conclusions

A series of perovskites with the general formula $Ln_{1-x}M_xCr_{0.9}Ni_{0.1}O_3$ (Ln = La and/or Nd; M = Sr and/or Ca; $x \leq 0.25$) has been prepared by the combustion method using glycine, urea and sucrose as combustible substances. The effect of doping x has been isolated from other lattice effects by fixing $< r_A >$ to 1.22 Å and $\sigma^2(r_A)$ to 0.0001 $Å^2$. At room temperature, all compounds show orthorhombic symmetry (S.G: *Pnma*) and the unit cell compresses as x increases. There is also a systematic increase in grain growth with doping, which is consistent with the introduction of increasing amounts of alkaline-earth cation, specially Ca, which is believe to form low temperature melting intermediate species that promote sintering.

The electrical conductivity measured in H_2 shows important dependences with x and with the synthetic method. Irrespective of x, conductivity is always higher in the following order: urea, glycine and sucrose. An interesting observation is that, upon doping, the electronic conductivity measured under hydrogen atmosphere decreases contrary to common expectations for a p-type doping of the oxide perovskites. This effect has not been reported before although there were some evidences that this could occur under reducing conditions at sufficiently low oxygen partial pressures. Moreover, this behavior is consistent with all literature works that report the increase of oxygen vacancy formation with x, which could be attributed to the lower charge density of the doping cations. As a consequence, only samples with lower doping values have conductivity values that are reasonable for a SOFC anode. Thermal expansion coefficients are also closer to that of the most common SOFC electrolyte (YSZ) for samples with lower x, which indicates that less doped phases are the only ones that reasonably meet the basic needs as anodes.

Acknowledgements

This research has been funded by the Ministerio de Economía y Competitividad (MAT2016-76739-R), the Feder program of the European Union and Dpto. Educación, Política Lingüística y Cultura of the Basque Government (IT-630-13). The authors thank for technical and human support provided by SGIker of UPV/EHU. L.Ortega-San-Martin acknowledges Departamento de Ciencias, PUCP (Peru), for funding two shorts stays at UPV/EHU.

Appendix A. Supporting information

Supplementary data associated with this article can be found in the online version at http://dx.doi.org/10.1016/j.ceramint.2017.10.182.

References

[1] N. Mahato, A. Banerjee, A. Gupta, S. Omar, K. Balani, Progress in material selection for solid oxide fuel cell technology: a review, Prog. Mater. Sci. 72 (2015) 141–337, http://dx.doi.org/10.1016/j.pmatsci.2015.01.001.

[2] W.-H. Kan, V. Thangadurai, Challenges and prospects of anodes for solid oxide fuel cells (SOFCs), Ion. 21 (2014) 301–318, http://dx.doi.org/10.1007/s11581-014-1334-6.

[3] D.K. Niakolas, Sulfur poisoning of Ni-based anodes for solid oxide fuel cells in H/C-based fuels, Appl. Catal. A Gen. 486 (2014) 123–142, http://dx.doi.org/10.1016/j.apcata.2014.08.015.

[4] J. Sunarso, S.S. Hashim, N. Zhu, W. Zhou, Perovskite oxides applications in high temperature oxygen separation, solid oxide fuel cell and membrane reactor: a review, Prog. Energy Combust. Sci. 61 (2017) 57–77, http://dx.doi.org/10.1016/j.pecs.2017.03.003.

[5] H. Teruhisa, LaCrO3-Based perovskite for SOFC interconnects, Perovskite Oxide Solid Oxide Fuel Cells (2009) 285–296, http://dx.doi.org/10.1007/978-0-387-77708-5.

[6] J.T.S. Irvine, Perovskite oxide anodes for SOFCs, in: T. Ishihara (Ed.), Perovskite Oxide Solid Oxide Fuel Cells, Springer Science, 2009, pp. 167–182, , http://dx.doi.org/10.1007/978-0-387-77708-5.

[7] S. Tao, J.T.S. Irvine, Discovery and characterization of novel oxide anodes for solid oxide fuel cells, Chem. Rec. 4 (2004) 83–95, http://dx.doi.org/10.1002/tcr.20003.

[8] N.P. Brandon, S. Skinner, B.C.H. Steele, Recent advances in materials for fuel cells, Annu. Rev. Mater. Res. 33 (2003) 183–213, http://dx.doi.org/10.1146/annurev.matsci.33.022802.094122.

[9] S. Gupta, H. Sabarou, Y. Zhong, P. Singh, Phase evolution and electrochemical performance of iron doped lanthanum strontium chromite in oxidizing and reducing atmosphere, Int. J. Hydrog. Energy 42 (2017) 6262–6271, http://dx.doi.org/10.1016/j.ijhydene.2016.11.141.

[10] T. Zhu, D.E. Fowler, K.R. Poeppelmeier, M. Han, S.A. Barnett, Hydrogen oxidation mechanisms on perovskite solid oxide fuel cell anodes, J. Electrochem. Soc. 163 (2016) F952–F961, http://dx.doi.org/10.1149/2.1321608jes.

[11] V.Y. Zenou, D.E. Fowler, R. Gautier, S.A. Barnett, K.R. Poeppelmeier, L.D. Marks, Redox and phase behavior of Pd-substituted (La,Sr)CrO3 perovskite solid oxide fuel cell anodes, Solid State Ion. 296 (2016) 90–105, http://dx.doi.org/10.1016/j.ssi.2016.09.006.

[12] J. Sfeir, LaCrO3-based anodes: stability considerations, J. Power Sources 118 (2003) 276–285, http://dx.doi.org/10.1016/S0378-7753(03)00099-5.

[13] O.V. Komova, V.I. Simagina, S.A. Mukha, O.V. Netskina, G.V. Odegova, O.A. Bulavchenko, A.V. Ishchenko, A.A. Pochtar, A modified glycine-nitrate combustion method for one-step synthesis of LaFeO3, Adv. Powder Technol. 27 (2016) 496–503, http://dx.doi.org/10.1016/j.apt.2016.01.030.

[14] S. Singh, D. Singh, LaSrFeO4 nanopowders synthesized by different combustion methods: effect of fuel/particle size, Ceram. Int. 42 (2016) 15725–15731, http://dx.doi.org/10.1016/j.ceramint.2016.07.032.

[15] D.P. Tarragó, C. de, F. Malfatti, V.C. de Sousa, Influence of fuel on morphology of LSM powders obtained by solution combustion synthesis, Powder Technol. 269 (2015) 481–487, http://dx.doi.org/10.1016/j.powtec.2014.09.037.

[16] F. Deganello, L.F. Liotta, G. Marcì, E. Fabbri, E. Traversa, Strontium and iron-doped barium cobaltite prepared by solution combustion synthesis: exploring a mixed-fuel approach for tailored intermediate temperature solid oxide fuel cell cathode materials, Mater. Renew. Sustain. Energy 2 (2013) 8, http://dx.doi.org/10.1007/s40243-013-0008-z.

[17] L.M. Rodriguez-Martinez, J.P. Attfield, Cation disorder and size effects in magnetoresistive manganese oxide perovskites, Phys. Rev. B 54 (1996) R15622–R15625.

[18] A.K. Kundu, M.M. Seikh, K. Ramesha, C.N.R. Rao, Novel effects of size disorder on the electronic and magnetic properties of rare earth manganates of the type La 0.7 − xLnxBa0.3MnO3 (Ln = Pr,Nd, Gd or Dy) with large average radius of the A-site cations, J. Phys. Condens. Matter 17 (2005) 4171–4180, http://dx.doi.org/10.1088/0953-8984/17/26/015.

[19] K. Vidal, A. Larrañaga, A. Morán-Ruiz, A.T. Aguayo, M.A. Laguna-Bercero, M.P. Yeste, J.J. Calvino, M.I. Arriortua, Effect of synthesis conditions on electrical and catalytical properties of perovskites with high value of A-site cation size mismatch, Int. J. Hydrog. Energy 41 (2016) 19810–19818, http://dx.doi.org/10.1016/j.ijhydene.2016.02.088.

[20] J.-G. Cheng, J.-S. Zhou, J.B. Goodenough, Lattice effects on ferromagnetism in perovskite ruthenates, Proc. Natl. Acad. Sci. USA 110 (2013) 13312–13315, http://dx.doi.org/10.1073/pnas.1311871110.

[21] A. Ecija, K. Vidal, A. Larrañaga, A. Martínez-Amesti, L. Ortega-San-Martín, M.I. Arriortua, Structure and properties of perovskites for SOFC cathodes as a function of the A-site cation size disorder, Solid State Ion. 235 (2013) 14–21, http://dx.doi.org/10.1016/j.ssi.2013.01.010.

[22] R.D. Shannon, Revised effective ionic radii and systematic studies of interatomie distances in halides and chaleogenides, Acta Cryst. A32 (1976) 751–767, http://dx.doi.org/10.1107/S0567739476001551.

[23] P.M. Woodward, Octahedral tilting in perovskites. I. Geometrical considerations, Acta Crystallogr. Sect. B Struct. Sci. 53 (1997) 32–43, http://dx.doi.org/10.1107/S0108768196010713.

[24] K. Oikawa, T. Kamiyama, T. Hashimoto, Y. Shimojyo, Y. Morii, Structural phase transition of orthorhombic LaCrO3 studied by neutron powder diffraction, J. Solid State Chem. 154 (2000) 524–529, http://dx.doi.org/10.1006/jssc.2000.8873.

[25] A.C. Larson, R.B. Von Dreele, General structure analysis system (GSAS), Los Alamos Lab. Rep. LAUR 86–74 (2004).

[26] B.H. Toby, EXPGUI, a graphical user interface for GSAS, J. Appl. Crystallogr. 34 (2001) 210–213, http://dx.doi.org/10.1107/S0021889801002242.

[27] L. Ortega-San-Martín, K. Vidal, B. Roldán-Pozo, Y. Coello, A. Larrañaga, M.I. Arriortua, Synthesis method dependence of the lattice effects in Ln0.5M0.5FeO3 perovskites (Ln = La and (Nd or Gd); M = Ba and (Ca or Sr)), Mater. Res. Express 3 (2016) 56302, http://dx.doi.org/10.1088/2053-1591/3/5/056302.

[28] A.L.A. Da Silva, G.G.G. Castro, M.M.V.M. Souza, Synthesis of Sr-doped LaCrO 3 powders by combustion method: influence of the fuel agent, J. Therm. Anal. Calorim. 109 (2012) 33–38, http://dx.doi.org/10.1007/s10973-011-1527-4.

[29] B.S. Barros, J. Kulesza, D.M. De. Arajo Melo, A. Kiennemand, Nickel-based catalyst

precursor prepared via microwave-induced combustion method: thermodynamics of synthesis and performance in dry reforming of CH4, Mater. Res. 18 (2015) 732–739, http://dx.doi.org/10.1590/1516-1439.018115.
[30] A.S. Mukasyan, C. Costello, K.P. Sherlock, D. Lafarga, A. Varma, Perovskite membranes by aqueous combustion synthesis: synthesis and properties, Sep. Purif. Technol. 25 (2001) 117–126, http://dx.doi.org/10.1016/S1383-5866(01)00096-X.
[31] S. Simner, J. Hardy, J. Stevenson, T. Armstrong, Sintering mechanisms in strontium doped lanthanum chromite, J. Mater. Sci. 34 (1999) 5721–5732, http://dx.doi.org/10.1023/A:1006733414271.
[32] S.W. Paulik, S. Baskaran, T.R. Armstrong, Mechanical properties of calcium- and strontium- substituted lanthanum chromite, J. Mater. Sci. 3 (1998) 2397–2404.
[33] S.R. Nair, R.D. Purohit, A.K. Tyagi, P.K. Sinha, B.P. Sharma, Role of glycine-to-nitrate ratio in influencing the powder characteristics of La(Ca)CrO3, Mater. Res. Bull. 43 (2008) 1573–1582, http://dx.doi.org/10.1016/j.materresbull.2007.06.021.
[34] J.T.S. Irvine, P. Connor, Alternative materials for SOFCs, opportunities and limitations, in: J.T.S. Irvine, P. Connor (Eds.), Solid Oxide Fuels Cells Facts Figures Past, Present Future Perspectives SOFC Technologies, Springer-Verlag, London, 2013, pp. 163–180, , http://dx.doi.org/10.1007/978-1-4471-4456-4_7.
[35] I. Yasuda, T. Hikita, Electrical conductivity and defect structure of calcium-doped lanthanum chromites, J. Electrochem. Soc. 140 (1993) 1699, http://dx.doi.org/10.1149/1.2221626.
[36] I. Yasuda, M. Hishinuma, Electrical conductivity and chemical diffusion coefficient of Sr-doped lanthanum chromites, Solid State Ion. 80 (1995) 141–150, http://dx.doi.org/10.1016/0167-2738(95)00136-T.
[37] S. Tao, J.T.S. Irvine, Structural and electrochemical properties of the perovskite oxide Pr0.7Sr0.3Cr0.9Ni0.1O3 − δ, Solid State Ion. 179 (2008) 725–731, http://dx.doi.org/10.1016/j.ssi.2008.04.027.
[38] S. Tao, J.T.S. Irvine, Phase transition in perovskite oxide La0.75Sr0.25Cr0.5Mn0.5O3-δ observed by in situ high-temperature neutron powder diffraction, Chem. Mater. 18 (2006) 5453–5460, http://dx.doi.org/10.1021/cm061413n.
[39] S.P. Jiang, L. Liu, K.P. Ong, P. Wu, J. Li, J. Pu, Electrical conductivity and performance of doped LaCrO3 perovskite oxides for solid oxide fuel cells, J. Power Sources 176 (2008) 82–89, http://dx.doi.org/10.1016/j.jpowsour.2007.10.053.
[40] D.P. Karim, A.T. Aldred, Localized level hopping transport in La(Sr)CrO3, Phys. Rev. B 20 (1979) 2255–2263, http://dx.doi.org/10.1103/PhysRevB.20.2255.
[41] N. Sakai, T. Kawada, H. Yokokawa, M. Dokiya, T. Iwata, Sinterability and electrical conductivity of calcium-doped lanthanum chromites, J. Mater. Sci. 25 (1990) 4531–4534, http://dx.doi.org/10.1007/BF00581119.
[42] L. Manxi, C. Xiangfeng, Z. Weichang, D. Yongping, C. Tongyun, Preparation and performance of Sm1-xCaxCrO3-δ as new interconnect materials for IT-SOFC, Rare Met. Mater. Eng. 43 (2014) 1337–1341, http://dx.doi.org/10.1016/S1875-5372(14)60119-3.
[43] K.J. Yoon, C.N. Cramer, E.C. Thomsen, C.A. Coyle, G.W. Coffey, O.A. Marina, Calcium- and cobalt-doped yttrium chromites as an interconnect material for solid oxide fuel cells, J. Electrochem. Soc. 157 (2010) B856–B861, http://dx.doi.org/10.1149/1.3337156.
[44] X.-M. Ge, S.-H. Chan, Q.-L. Liu, Q. Sun, Solid oxide fuel cell anode materials for direct hydrocarbon utilization, Adv. Energy Mater. 2 (2012) 1156–1181, http://dx.doi.org/10.1002/aenm.201200342.
[45] N. Sakai, H. Yokokawa, T. Horita, K. Yamaji, Lanthanum chromite-based interconnects as key materials for SOFC stack development, Int. J. Appl. Ceram. Technol. 1 (2004) 23–30, http://dx.doi.org/10.1111/j.1744-7402.2004.tb00151.x.
[46] J. Mizusaki, Y. Yonemura, H. Kamata, K. Ohyama, N. Mori, H. Takai, H. Tagawa, M. Dokiya, K. Naraya, T. Sasamoto, H. Inaba, T. Hashimoto, Electronic conductivity, seebeck coefficient, defect and electronic structure of nonstoichiometric La1 − xSrxMnO3, Solid State Ion. 132 (2000) 167–180, http://dx.doi.org/10.1016/S0167-2738(00)00662-7.
[47] J. Mizusaki, J. Tabuchi, T. Matsuura, S. Yamauchi, K. Fueki, Electrical conductivity and seebeck coefficient of nonstoichiometric La1 − xSrxCoO3 − δ, J. Electrochem. Soc. 136 (1989) 2082–2088, http://dx.doi.org/10.1149/1.2097187.
[48] J. Mizusaki, S. Yamauchi, K. Fueki, A. Ishikawa, Nonstoichiometry of the perovskite-type oxide La1 − xSrxCrO3 − δ, Solid State Ion. 12 (1984) 119–124, http://dx.doi.org/10.1016/0167-2738(84)90138-3.
[49] F. Boroomand, E. Wessel, H. Bausinger, K. Hilpert, Correlation between defect chemistry and expansion during reduction of doped LaCrO3 interconnects for SOFCs, Solid State Ion. 129 (2000) 251–258, http://dx.doi.org/10.1016/S0167-2738(99)00330-6.
[50] J.E. Huheey, E.A. Keiter, R.L. Keiter, Inorganic Chemistry: Principles of Structure and Reactivity, 4th ed., Harper Collins College Publishers, New York, 1993.
[51] M.K. Rath, K.T. Lee, Investigation of aliovalent transition metal doped La0.7Ca0.3Cr0.8 × 0.2O3-δ (X = Ti, Mn, Fe, Co, and Ni) as electrode materials for symmetric solid oxide fuel cells, Ceram. Int. 41 (2015) 10878–10890, http://dx.doi.org/10.1016/j.ceramint.2015.05.029.
[52] V.V. Kharton, F.M.B. Marques, A. Atkinson, Transport properties of solid oxide electrolyte ceramics: a brief review, Solid State Ion. 174 (2004) 135–149, http://dx.doi.org/10.1016/j.ssi.2004.06.015.